Theoretical Investigation of Electron Paramagnetic Resonance Spectra and Local Structure Distortion for Mn^{2+} Ions in $CaCO_3$:Mn^{2+} System: A Simple Model for Mn^{2+} Ions in a Trigonal Ligand Field

Lu Cheng,[†] Kuang Xiao-Yu,*[,†,‡] Tan Xiao-Ming,[†] and Yang Xiong[†]

Institute of Atomic and Molecular Physics, Sichuan University, Chengdu 610065, China, and International Centre for Materials Physics, Academia Sinica, Shenyang 110016, China

Received: October 31, 2006; In Final Form: January 14, 2007

This paper reports on a novel application of a ligand field model for the detection of the local molecular structure of a coordination complex. By diagonalizing the complete energy matrices of the electron−electron repulsion, the ligand field and the spin−orbit coupling for the d^5 configuration ion in a trigonal ligand field, the local distortion structure of the $(MnO_6)^{10-}$ coordination complex for Mn^{2+} ions doped into $CaCO_3$, have been investigated. Both the second-order zero-field splitting parameter b_2^0 and the fourth-order zero-field splitting parameter b_4^0 are taken simultaneously in the structural investigation. From the electron paramagnetic resonance (EPR) calculations, the local structure distortion, $\Delta R = -0.169$ Å to -0.156 Å, $\Delta\theta = 0.996°$ to $1.035°$ for Mn^{2+} ions in calcite single crystal, $\Delta R = -0.185$ Å to -0.171 Å, $\Delta\theta = 3.139°$ to $3.184°$ for Mn^{2+} ions in travertines, and $\Delta R = -0.149$ Å to -0.102 Å, $\Delta\theta = 0.791°$ to $3.927°$ for Mn^{2+} ions in shells are determined, respectively. These results elucidate a microscopic origin of various ligand field parameters which are usually used empirically for the interpretation of EPR and optical absorption experiments. It is found that the theoretical results of the EPR and optical absorption spectra for Mn^{2+} ions in $CaCO_3$ are in good agreement with the experimental findings. Moreover, to understand the detailed physical and chemical properties of the doped $CaCO_3$, the theoretical values of the fourth-order zero-field splitting parameters b_4^0 for Mn^{2+} ions in travertines and shells are reported first.

I. Introduction

Impurities in solid materials have been a subject of widespread interest in recent years as doped materials can display new properties which are absent in pure compounds.[1,2] Among the impurities, particular attention has been focused on the transition-metal ions.[3−6] The transition-metal divalent manganese ion is perhaps the most investigated impurity ion because the shell of 3d electrons responsible for the paramagnetism is just half filled by the five electrons, and the resultant orbital angular momentum is 0.[4−6] Since the total spin is 5/2, it exhibits an additional interaction, the zero-field splitting, and this splitting is highly sensitive to the local structure of manganese centers. Electron paramagnetic resonance (EPR) is regarded as an effective tool to study the microstructure and the local environment around a substitution magnetic ion site in crystals.[7,8] The reason is that the EPR spectra usually provide highly detailed microscopic information about the structure of the defects. The EPR spectrum of the Mn^{2+} paramagnetic ions was used to study the local structure distortions,[9] the structural phase transitions,[10,11] the existence of a high-spin to low-spin transition,[12] and the radicals produced during reaction processes in proteins[13] and other biomacromolecules.[14−18] So, we can study the local environments of Mn^{2+} ions from their EPR data.

The EPR spectra of transition-metal Mn^{2+} ions doped into $CaCO_3$ have been experimentally observed by many researchers.[19−25] These experimental results give important information about the ground state of the transition-metal Mn^{2+} ions and form a useful starting point for understanding the interrelationships between electronic and molecular structure of Mn^{2+} ions in the $(MnO_6)^{10-}$ coordination complex. However, so far, there has been no systematical theory for their analysis. The reason why the previous theoretical results are not quite in good agreement with the observed values may be due to the oversimplification of the theoretical method. For instance, Zheng[26] has theoretically investigated the $CaCO_3$:Mn^{2+} system in single crystal by the superposition model. But in Zheng's work,[26] the calculations of the zero-field splitting parameters b_2^0 and b_4^0 are not in good agreement with the experiment values, which may be ascribed to the fact that the approximate formulas $R \approx (R_H + R_P)/2$ and $\theta \approx (\theta_H + \theta_P)/2$ were taken in the structural investigation. According to the point-charge model and the superposition model, Yu and Zhao have made a theoretical investigation of the second-order zero-field splitting parameter b_2^0 for Mn^{2+} ions in the $CaCO_3$:Mn^{2+} system by using the fourth-order and the sixth-order perturbation formulas.[27] However, they did not investigate the fourth-order zero-field splitting parameters b_4^0 of Mn^{2+} ions in the $CaCO_3$:Mn^{2+} system.

It is well-known that for a d^5 configuration ion in a trigonal ligand field, the high-spin ground state is the $^6A_1$ state. To describe the $^6A_1$ ground-state splitting of the Mn^{2+} ions in the $CaCO_3$:Mn^{2+} system, the spin Hamiltonian should include three different zero-field splitting parameters b_2^0, b_4^0, and b_4^3. The parameter b_4^3 relates to a fourth-order spin operator and represents a cubic component of the crystalline electric field. The parameters b_2^0 and b_4^0 are respectively associated with the second-order and fourth-order spin operators and represent an

* Corresponding author. E-mail: palc@163.com.
† Sichuan University.
‡ Academia Sinica.

10.1021/jp067161v CCC: $37.00
Published on Web 03/09/2007

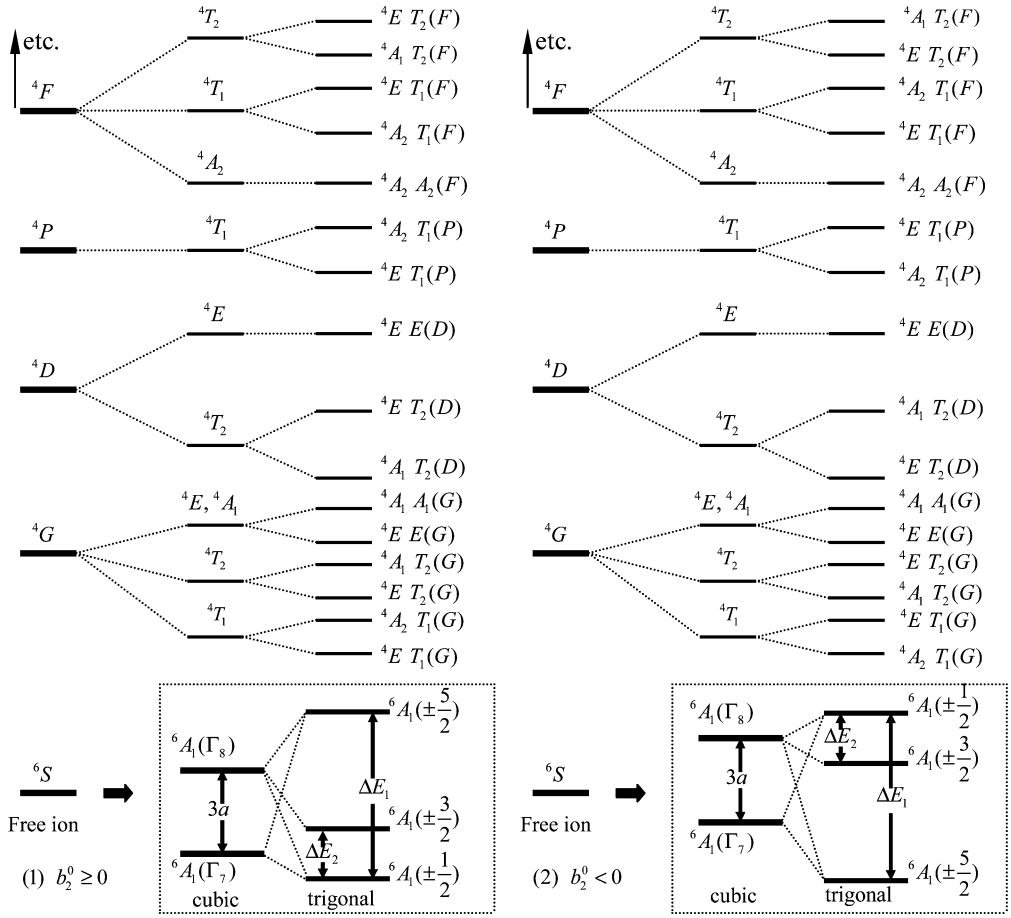

Figure 1. Splitting of the energy levels for the Mn^{2+} ion in the crystal field of trigonal symmetry. a is the cubic field splitting parameter, $\Delta E_1 = \pm 1/3[(18b_2^0 - 3b_4^0)^2 + 9/10(b_4^3)^2]^{1/2}$ and $\Delta E_2 = -b_2^0 - (9/2)b_4^0 \pm 1/6[(18b_2^0 - 3b_4^0)^2 + 9/10(b_4^3)^2]^{1/2}$ are the zero-field splitting energies in the ground state $^6A_1$. The positive and negative signs correspond to $b_2^0 \geq 0$ and $b_2^0 < 0$, respectively.[32]

axial component of the crystalline electric field that is axially symmetric about the C_3 axis. In order to explain more reasonably structure distortion, herein, we suggest that the two zero-field splitting parameters b_2^0 and b_4^0 should be simultaneously considered in the determination of the local structure distortion of Mn^{2+} ions in the $CaCO_3$:Mn^{2+} system. In the present work, a theoretical model for determining the local structure distortion of Mn^{2+} ions in the $(MnO_6)^{10-}$ coordination complex is proposed by diagonalizing the complete energy matrices for the d^5 configuration ion in a trigonal ligand field and by considering the second-order and fourth-order zero-field splitting parameters b_2^0 and b_4^0 simultaneously. By this model, the optical absorption and EPR spectra of Mn^{2+} ions in calcite single crystal, travertines and shells have been investigated.

II. Ligand Field Model

Firstly, we construct the complete energy matrix of the d^5 configuration ion within the ligand field scheme. There are two different ways which have been developed to construct the complete matrix. One way is Racah's method, in which the tensor operator has been used;[28] the other way is Slater's method, in which the relationships between the matrix of the single d electron and the matrix of the d^n configuration have been established.[29] In the present work, Slater's method has been employed. For a d^5 configuration ion in a trigonal ligand field, in order to construct the complete matrixes, the $|J,M_J\rangle$ basic functions need to expand into the form of the $|L,S,M_L,M_S\rangle_i$ basic functions. This expansion may be realized in terms of the Clebsch−Gordon coefficients which are associated with the coupling of two angular moments. In general, the expansion can be written as[30]

$$\psi_{jm} = \sum_{m_1 m_2} (j_1 j_2 m_1 m_2 | j_1 j_2 jm) \psi_{j_1 m_1} \psi_{j_2 m_2} = \sum_{m_1 m_2} \left\{ \delta_{m,m_1+m_2} \times \left[(2j+1) \frac{(j+j_1-j_2)!(j-j_1+j_2)!(j_1+j_2-j)!}{(j+j_1+j_2+1)!} \times (j_1+m_1)! (j_1-m_1)!(j_2+m_2)!(j_2-m_2)!(j+m)!(j-m)! \right]^{1/2} \times \sum_{\gamma} \frac{(-1)^{\gamma}}{\gamma!} [(j_1+j_2-j-\gamma)!(j_1-m_1-\gamma)!(j_2+m_2-\gamma)! \times (j-j_2+m_1+\gamma)!(j-j_1-m_2+\gamma)!]^{-1} \right\} \psi_{j_1 m_1} \psi_{j_2 m_2} \quad (1)$$

The relationship of the coefficients between m and $-m$ is

$$\langle j_1 j_2 m_1 m_2 | j_1 j_2 jm \rangle = (-1)^{j_1+j_2-j} \langle j_1 j_2 - m_1 - m_2 | j_1 j_2 j - m \rangle \quad (2)$$

From eqs 1 and 2, it is easy to get the $|J,M_J\rangle$ basic functions

$$|J,M_J\rangle = \sum_i C_i |L,S,M_L,M_S\rangle_i = \sum_i \sum_j C_i C_j \Phi_j \quad (3)$$

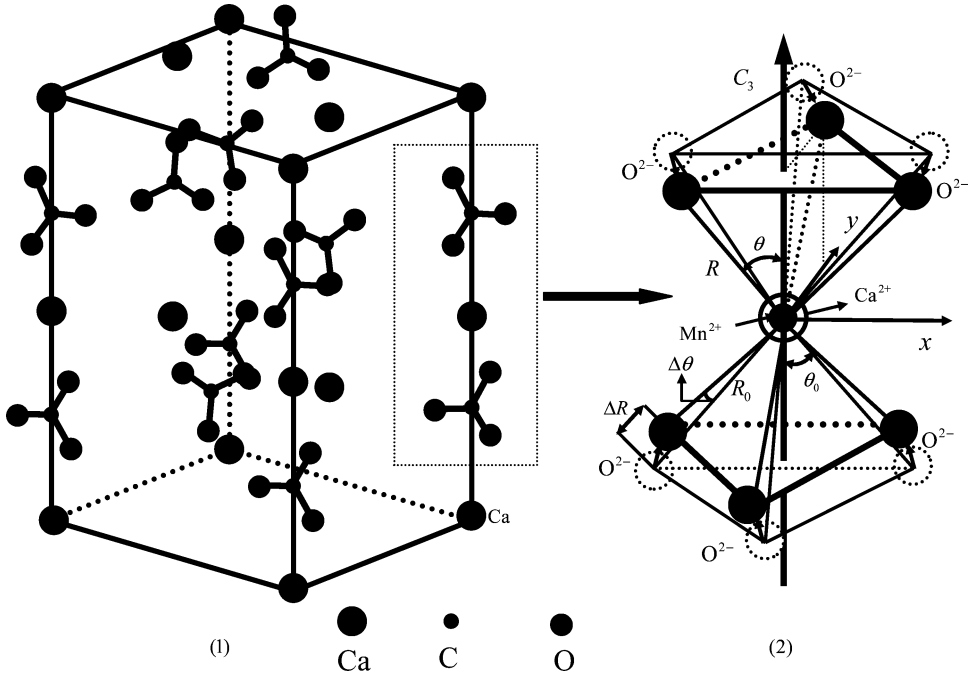

Figure 2. (1) Rhombohedral unit cell of calcite. (2) Local structure distortion for Mn^{2+} ions in the $CaCO_3$:Mn^{2+} system. R_0 and θ_0 are the structure parameters of $CaCO_3$. ΔR and $\Delta\theta$ represent the structure distortion. R is the Mn−O bond lengths. θ is the angle between the Mn−O bond and the C_3 axis when the Mn^{2+} ion replaces the Ca^{2+} ion.

where C_i and C_j are the Clebsch−Gordon coefficients and Φ_j is one of the 252 basic Slater determinants. According to the $|L,S,M_L,M_S\rangle_i$ functions of the d^5 configuration ion in a trigonal ligand field, we have constructed the complete energy matrix of the Hamiltonian

$$\hat{H} = \hat{H}_{ee} + \hat{H}_{so} + \hat{H}_{lf} = \sum_{i<j} e^2/r_{i,j} + \zeta \sum_i l_i \cdot s_i + \sum_i V_i \quad (4)$$

where the first term is the electron−electron interactions, the second term is the spin−orbit coupling interactions, and the third term is the ligand field potentials. For a d^5 configuration ion in a trigonal ligand field, there are 252 independent wave functions. Using the $|J,M_J\rangle$ functions, we find that the symmetry-adapted functions for the C_3^* double group can be divided into three groups associated with the Γ_1 (or Γ_3), Γ_2, and Γ_4 representations, respectively. From the representations, three 84 × 84 matrices have been constructed. The matrix elements are the function of the Racah parameters B and C, Tree's correction α, Racah's correction β, the spin−orbit coupling coefficient ζ, and the ligand field parameters B_{20}, B_{40}, B_{43}^c, and B_{43}^s which are in the following forms[31]

$$B_{20} = \frac{1}{2}\sum_\tau G_2(\tau)(3\cos^2\theta_\tau - 1)$$

$$B_{40} = \frac{1}{8}\sum_\tau G_4(\tau)(35\cos^4\theta_\tau - 30\cos^2\theta_\tau + 3)$$

$$B_{43}^c = \frac{\sqrt{35}}{4}\sum_\tau G_4(\tau)(\sin^3\theta_\tau\cos\theta_\tau\cos 3\phi_\tau)$$

$$B_{43}^s = i\frac{\sqrt{35}}{4}\sum_\tau G_4(\tau)(\sin^3\theta_\tau\cos\theta_\tau\sin 3\phi_\tau) \quad (5)$$

The EPR spectra of d^5 configuration Mn^{2+} ions in a trigonal ligand field may be analyzed by employing the spin Hamiltonian[32]

$$\hat{H} = \mu_B \vec{B}\cdot\vec{g}\cdot\vec{S} + \frac{1}{3}b_2^0 O_2^0 + \frac{1}{60}(b_4^0 O_4^0 + b_4^3 O_4^3) \quad (6)$$

where the first term corresponds to the Zeeman interaction and the following terms represent the zero-field interaction. μ_B is the Bohr magneton, $\vec{B}$ is the magnetic field, $\vec{g}$ is the splitting factor, $\vec{S}$ is the spin angular momentum operator, O_k^q are the standard Stevens spin operators,[33] and b_k^q are the zero-field splitting parameters. From the spin Hamiltonian, we can easily obtain the zero-field splitting energy levels ΔE_1 and ΔE_2 in the ground state $^6A_1$ for a zero-magnetic field.[32] These energy levels are given in Figure 1.

III. Local Structure Distortion for Mn^{2+} Ions in the $(MnO_6)^{10-}$ Coordination Complex

A. Calculation for Mn^{2+} Ions in Calcite and Travertine. The crystallographic properties of calcite are well-studied.[34,35] Calcite is the rhombohedral form of $CaCO_3$ and belongs to the space group D_{3d}^6. There are two nonequivalent Ca^{2+} sites in the calcite structure associated with the alternation of the carbonate ion orientations in successive carbonate planes. When the divalent Mn^{2+} ion is doped into calcite, it will substitute for the Ca^{2+} ion site. The Mn^{2+} ion is octahedrally coordinated to six nearest-neighbor O atoms of the CO_3^{2-} ions. In order to describe the distortion, the Z axis is chosen along the threefold axis, as shown in Figure 2. According to the superposition model,[36] the ligand field parameter B_{43}^s in eq 5

TABLE 1: Observed and Calculated Optical Absorption Spectra for Mn^{2+} Ions in $MnCO_3$, $MnCl_2$, $MnBr_2$, and MnI_2 Compounds[a]

	$MnCO_3$ (4.2 K)		$MnCl_2$ (78 K)		$MnBr_2$ (78 K)		MnI_2 (5 K)	
state	obsd[b]	calcd	obsd[c]	calcd	obsd[c]	calcd	obsd[d]	calcd
$^4T_1(G)$	18350	18349.9	18500	18499.5	18450	18450.2	17630	17630.8
$^4T_2(G)$	22600	22591.4	22000	21989.1	21650	21636.7	20600	20587.9
$^4A_1(G)$	24580	24579.5	23590	23589.7	23084	23087.1	22373	22376.2
$^4E(G)$	24580	24579.5	23825	23589.7	23550	23087.1	22062	22376.2
$^4T_2(D)$	27255	27284.1	26750	26778.3	26520	26516.1	25420	25430.6
$^4E(D)$	29170	29210.0	28065	28076.8	27505	27530.9	26338	26373.9
$^4T_1(P)$	31900	31947.7	36500	36534.8	29950	29987.8	28920	28992.7
$^4A_2(F)$	36500	36553.4	38400	38435.9	34800	34854.1		32725.7
$^4T_1(F)$	40820	40865.8	40650	40692.1	37400	37458.2		36958.6
$^4T_2(F)$	41670	41697.5	42370	42410.2	38750	38773.6		37634.3

[a] All levels in units of cm^{-1}. [b] Reference 39. [c] Reference 41. [d] Reference 42.

TABLE 2: Calculated Parameters for Mn^{2+} in $MnCO_3$, $MnCl_2$, $MnBr_2$, and MnI_2 Compounds

parameters	N	B (cm^{-1})	C (cm^{-1})	α (cm^{-1})	β (cm^{-1})	Dq (cm^{-1})	A_2 (au)	A_4 (au)
$MnCO_3$	0.9782	840.53	2996.79	59.51	−119.94	771.7	3.056056	25.610553
$MnCl_2$	0.9682	806.68	2876.12	57.12	−115.11	646.6	5.889934	49.359155
$MnBr_2$	0.9630	789.49	2814.82	55.90	−112.66	596.1	6.963984	58.359967
MnI_2	0.9555	765.18	2728.15	54.18	−109.19	604.5	10.174621	85.269530

will vanish, and the parameters $G_2(\tau)$ and $G_4(\tau)$ can be derived as[37]

$$G_2(\tau) = eq_\tau G^2(\tau)$$

$$G_4(\tau) = eq_\tau G^4(\tau)$$

$$G^k(\tau) = \int_0^R R_{3d}{}^2(r) r^2 \frac{r^k}{R^{k+1}}\,dr + \int_R^\infty R_{3d}{}^2(r) r^2 \frac{R^k}{r^{k+1}}\,dr \quad (7)$$

According to the Van Vleck approximation for the $G^k(\tau)$ integral,[37] we may obtain the following relations

$$G_2(\tau) = \frac{-eq_\tau\langle r^2\rangle}{R^3} = \frac{A_2}{R^3}, \qquad G_4(\tau) = \frac{-eq_\tau\langle r^4\rangle}{R^5} = \frac{A_4}{R^5} \quad (8)$$

where $A_2 = -eq_\tau\langle r^2\rangle$, $A_4 = -eq_\tau\langle r^4\rangle$, and $A_2/A_4 = \langle r^2\rangle/\langle r^4\rangle$. The ratio of $\langle r^2\rangle/\langle r^4\rangle = 0.119\,328$ is obtained from the radial wave function of the Mn^{2+} ion in complexes.[38] A_4, as a constant for the $(MnO_6)^{10-}$ coordination complex, can have its value determined from the optical absorption spectra and the Mn−O bond length of the $MnCO_3$ crystal.[39,40] By fitting the calculated optical absorption spectra to the observed values, we can obtain different optical parameters for different Mn^{2+} compounds.[39,41−43] The quantitative calculation results are listed in Tables 1 and 2. From Table 2, we can see that $A_4(MnO_6)^{10-} < A_4(MnCl_6)^{4-} < A_4(MnBr_6)^{4-} < A_4(MnI_6)^{4-}$ for Mn^{2+} ions in the coordination complex. As to Mn^{2+} ions in calcite and travertine, we take $N = 0.9782$ in the calculation from the optical spectra of $MnCO_3$, since they have the similar structure and the same type of ligand. Thus, substituting $A_4 = 25.610\,553$ au and $A_2 = 3.056\,056$ au for Mn^{2+} ions in the $(MnO_6)^{10-}$ coordination complex into eqs 7 and 8, the local distortion structure of Mn^{2+} ions in calcite single crystal and travertine can be determined by diagonalizing the complete energy matrices. The local structure distortion can be described by two parameters ΔR and $\Delta\theta$ (see Figure 2). We used the following relationship to evaluate the bond length R and bond angle θ for Mn^{2+} ions in $CaCO_3$.

$$R = R_0 + \Delta R, \qquad \theta = \theta_0 + \Delta\theta \quad (9)$$

TABLE 3: Ground-State Zero-Field Splitting ΔE_1, ΔE_2, and the EPR Parameters b_2^0 and b_4^0 for Mn^{2+} Ions in Calcite Single Crystal at Room Temperature[a]

ΔR (Å)	$\Delta\theta$ (deg)	$10^4\Delta E_1$	$10^4\Delta E_2$	$10^4 b_2^0$	$10^4 b_4^0$
−0.116	0.85	−455.99	−143.09	−76.24	−1.93
−0.116	0.855	−453.89	−142.50	−75.88	−1.90
−0.116	0.86	−451.70	−141.49	−75.53	−1.96
−0.156	0.99	−457.40	−141.69	−76.54	−2.33
−0.156	**0.996**	**−454.29**	**−140.49**	**−76.03**	**−2.36**
−0.156	1.01	−447.59	−138.30	−74.91	−2.35
−0.196	1.12	−458.81	−139.10	−76.83	−2.96
−0.196	1.127	−454.29	−137.81	−76.12	−2.94
−0.196	1.14	−446.79	−135.19	−74.88	−2.96
exptl[b]		**−453.90**	**−140.39**	**−75.96**	**−2.36**
−0.169	1.025	−460.32	−141.72	−77.06	2.53
−0.169	**1.035**	**−456.83**	**−140.44**	**−76.48**	**2.55**
−0.169	1.045	−449.71	−138.13	−75.29	2.54
exptl[c]		**−456.65**	**−140.40**	**−76.45**	**−2.55**

[a] $10^4\Delta E_1$, $10^4\Delta E_2$, $10^4 b_2^0$, and $10^4 b_4^0$ are in units of cm^{-1}. [b] Reference 24. [c] Reference 25.

where $R_0 = 2.36$ Å and $\theta_0 = 52.8°$.[39,44] Thus, the trigonal ligand field parameters (B_{20}, B_{40}, and B_{43}^c) are only functions of ΔR and $\Delta\theta$. In order to decrease the number of adjustable parameters and reflect the covalency effects, we use Curie et al.'s covalent theory[45] and take an average covalence factor N to determine the optical parameters as follows

$$B = N^4 B_0, \qquad C = N^4 C_0, \qquad \alpha = N^4\alpha_0, \qquad \beta = N^4\beta_0, \qquad \zeta = N^2\zeta_0 \quad (10)$$

The values of the free-ion parameters for Mn^{2+} ions have been obtained as $B_0 = 918\ cm^{-1}$, $C_0 = 3273\ cm^{-1}$, $\alpha = 65\ cm^{-1}$, $\beta = -131\ cm^{-1}$, and $\zeta_0 = 347\ cm^{-1}$.[46] For Mn^{2+} ions in calcite single crystal and travertines, by diagonalizing the complete energy matrices, the ground-state zero-field splitting can be calculated with use of distortion parameters ΔR, $\Delta\theta$, and the covalence factor N. The comparisons between the theoretical values and the experimental findings are shown in Tables 3 and 4.

B. Calculation for Mn^{2+} Ions in Shells. Sea shell is mainly composed of two common mineral forms of $CaCO_3$, calcite and aragonite. It also consists of less amounts of $MgCO_3$, $Ca_3P_2O_8$,

TABLE 4: Ground-State Zero-Field Splitting ΔE_1, ΔE_2, and the EPR Parameters b_2^0 and b_4^0 for Mn^{2+} Ions in Travertines[a]

travertine samples	ΔR (Å)	$\Delta\theta$ (deg)	$10^4\Delta E_1$	$10^4\Delta E_2$	$10^4 b_2^0$	$10^4 b_4^0$ [b]	$10^4 b_2^0$ exptl[c]
ascagnano	−0.171	3.139	568.20	200.61	94.23	−2.39	94.21
massa martana	−0.185	3.184	622.62	219.61	103.28	−2.57	103.27
papigno	−0.179	3.164	598.83	211.20	99.21	−2.52	99.25
perugia	−0.177	3.165	593.49	209.41	98.44	−2.47	98.42
poggio moiano	−0.176	3.167	592.00	208.82	98.19	−2.45	98.22
postignano	−0.174	3.152	580.79	204.89	96.33	−2.41	96.36
sasso	−0.171	3.139	568.20	200.61	94.23	−2.39	94.21

[a] $10^4\Delta E_1$, $10^4\Delta E_2$, $10^4 b_2^0$, and $10^4 b_4^0$ are in units of cm^{-1}. [b] EPR parameters $10^4 b_4^0$ from −2.57 to −2.39 for Mn^{2+} ions in travertines are predicted first. The experimental values of $10^4 b_4^0$ from −2.55 to −2.36 for Mn^{2+} ions in calcite single crystal were reported in refs 24 and 25. [c] Reference 20.

TABLE 5: Observed and Calculated Optical Absorption Spectra for Mn^{2+} Ions in Shells[a]

	shell		operculum		arca burnesi		lamellidens marginalls	
state	obsd[b]	cald[b]	obsd[c]	calcd[c]	obsd[d]	calcd[d]	obsd[e]	calcd[e]
$^4T_1(G)$	17695	17694.7	18000	17999.6	17725	17724.6	17850	17849.5
$^4T_2(G)$	21270	21210.9	21280	21213.6	22069	22099.9	21735	21703.9
$^4A_1(G)$	22620	22620.7	23475	23473.1	24443	24443.1	24385	24385.1
$^4E(G)$	22620	22620.7	23475	23473.1	24443	2443.1	24385	24385.1
$^4T_2(D)$	26310	26372.6	25965	26059.4	26659	27683.4	27015	27066.9
$^4E(D)$	27391	27428.4	27170	27227.8	28081	28152.0	28565	28591.3
$^4T_1(P)$		29131.1		28978.6		30232.1	32250	32311.9
$^4A_2(F)$		31760.2		31203.3		32676.9		37834.7
$^4T_1(F)$		35393.4		34893.8		36421.7		39627.5
$^4T_2(F)$		39562.3		38893.9		41046.1		42148.8

[a] All levels in units of cm^{-1}. [b] Reference 48, $N = 0.9581$, $B = 773.55$ cm^{-1}, $C = 2757.97$ cm^{-1}, $\alpha = 54.77$ cm^{-1}, $\beta = -110.37$ cm^{-1}, $Dq = 624.8$ cm^{-1}. [c] Reference 48, $N = 0.9670$, $B = 802.69$ cm^{-1}, $C = 2861.88$ cm^{-1}, $\alpha = 56.84$ cm^{-1}, $\beta = -114.55$ cm^{-1}, $Dq = 686.7$ cm^{-1}. [d] Reference 50, $N = 0.9768$, $B = 835.73$ cm^{-1}, $C = 2979.67$ cm^{-1}, $\alpha = 59.17$ cm^{-1}, $\beta = -119.26$ cm^{-1}, $Dq = 822.5$ cm^{-1}. [e] Reference 51, $N = 0.9763$, $B = 834.02$ cm^{-1}, $C = 2973.58$ cm^{-1}, $\alpha = 59.05$ cm^{-1}, $\beta = -119.02$ cm^{-1}, $Dq = 803.0$ cm^{-1}.

TABLE 6: Ground-State Zero-Field Splitting ΔE_1, ΔE_2, and the EPR Parameters b_2^0 and b_4^0 for Mn^{2+} Ions in Shells[a]

	pila globosa			mytilus conradinus	mytilus edulis
shell layers	hypostracum	ostracum of operculum	hypostracum of operculum	prismatic layer	prismatic layer
ΔR (Å)	−0.144	−0.149	−0.148	−0.102	−0.109
$\Delta\theta$ (deg)	3.483	3.927	3.875	0.791	0.931
$10^4\Delta E_1$	704.80	903.19	878.41	−538.50	−481.82
$10^4\Delta E_2$	246.01	312.50	304.01	−168.40	−149.31
$10^4 b_2^0$	117.02	150.08	145.96	−90.08	−80.63
$(10^4 b_4^0)^b$	−2.36	−2.44	−2.39	−2.41	−2.43
$(10^4 b_2^0)_{expt}$	117[c]	150[c]	146[c]	−90[d]	−80.58[e]

[a] $10^4\Delta E_1$, $10^4\Delta E_2$, $10^4 b_2^0$, and $10^4 b_4^0$ are in units of cm^{-1}. [b] EPR parameters $10^4 b_4^0$ from −2.44 to −2.36 for Mn^{2+} ions in shells are predicted first. The experimental values of $10^4 b_4^0$ from −2.55 to −2.36 for Mn^{2+} ions in calcite single crystal were reported in refs 24 and 25. [c] Reference 48. [d] Reference 49. [e] Reference 47.

SiO_2, $(Al, Fe)_2O_3$, $CaSO_4$, protein, and mucopolysaccharides.[47] The EPR spectra of transition-metal Mn^{2+} ions in sea shells have been extensively studied by many researchers.[47−51] Blanchard and Chasteen observed that the local structure of Mn^{2+} ions in sea shell has a D_{3d} symmetry.[47] Thus, from the optical absorption spectra of Mn^{2+} ions in sea shell, we obtain that $N = 0.9581$ for Mn^{2+} ions in shell and $N = 0.9670$ for Mn^{2+} ions in operculum.[48] For the sake of simplicity, the results are given in Table 5. Substituting the covalence factor N into eq 10, we can get the optical parameters $B = 773.55$ cm^{-1}, $C = 2757.97$ cm^{-1}, $\alpha = 54.77$ cm^{-1}, $\beta = -110.37$ cm^{-1}, and $\zeta = 318.53$ cm^{-1} for Mn^{2+} ions in shell and $B = 802.69$ cm^{-1}, $C = 2861.88$ cm^{-1}, $\alpha = 56.84$ cm^{-1}, $\beta = -114.54$ cm^{-1}, and $\zeta = 324.48$ cm^{-1} for Mn^{2+} ions in operculum. By using eqs 5 and 6 and the optical parameters B, C, α, β, and ζ, we can calculate the corresponding local structure distortion parameters ΔR and $\Delta\theta$ by diagonalizing the complete energy matrices of the electron−electron repulsion, the ligand field, and the spin−orbit coupling of the d^5 configuration ion in a trigonal ligand field. The results are listed in Table 6.

It can be seen from Tables 3−6 that the theoretical results are in good agreement with the experimental values. From the calculation, the local lattice structures $R = 2.191-2.204$ Å, $\theta = 53.796-53.853°$ for Mn^{2+} ions in calcite single crystal, $R = 2.175-2.189$ Å, $\theta = 55.939-55.984°$ for Mn^{2+} ions in travertines, and $R = 2.211-2.258$ Å, $\theta = 53.591-56.727°$ for Mn^{2+} ions in shells are determined. These theoretical results may provide a satisfactory and unified explanation for the experimental findings of the optical absorption and EPR spectra. From the above studies, we can find that the local lattice structure of the $(MnO_6)^{10-}$ coordination complex for Mn^{2+} ions in the $CaCO_3$:Mn^{2+} system has a compressed distortion, $\Delta R < 0$ and $\Delta\theta > 0$. This compressed distortion may be attributed to the fact that the Mn^{2+} ion has an obviously smaller ionic radius ($r_{Mn^{2+}} = 0.91$ Å) than that of the Ca^{2+} ion ($r_{Ca^{2+}} = 1.00$ Å).[52] It should be also noted that the local lattice structure of the $CaCO_3$:Mn^{2+} system in travertines and shells are obviously different from those in calcite single crystal. This result may be explained by the external environmental factor, such as the density of the Mn^{2+} ions in water and the temperature of the

water. Of course, other factors can also affect the local structure, such as deposition and infiltration of clay minerals, dissolution and recrystallization cycles of $CaCO_3$, impurity of the protein and mucopolysaccharides, and biological action.

Using the complete diagonalization method, we establish the inter-relationships between electronic and molecular structure and study the local molecular structure of the $(MnO_6)^{10-}$ coordination complex. By comparing our theoretical results ($R = 2.191-2.204$ Å, $\theta = 53.796-53.853°$) with the results ($R = 2.29$ Å, $\theta = 53.46°$) obtained by Zheng,[26] we find it noteworthy to mention that the empirical formulas $R \approx (R_H + R_P)/2$ and $\theta \approx (\theta_H + \theta_P)/2$ are not suitable for the $CaCO_3$:Mn^{2+} system. Furthermore, the previous theoretical result of the second-order zero-field splitting parameter b_2^0 ($b_2^0 = -82 \times 10^{-4}$ cm^{-1}) obtained by Yu and Zhao[27] is not quite in good agreement with the observed value ($b_2^0 = -75.96 \times 10^{-4}$ cm^{-1}) for Mn^{2+} ions in the $CaCO_3$:Mn^{2+} system.[24] This indicates that the high-order perturbation method is imperfect. Considering that the two zero-field splitting parameters are useful in understanding the coupling strength of Mn^{2+} ions to the $CaCO_3$ lattice and accordingly in understanding the changes of other properties induced by the Mn^{2+} impurity, we have constructed the complete energy matrixes for d^5 configuration ion in a trigonal ligand field and have made an analysis of the zero-field splitting parameters b_2^0 and b_4^0 of Mn^{2+} ions in the $CaCO_3$:Mn^{2+} system. This is a generic theoretical method. It is very interesting as the complete diagonalization method avoids perturbation solutions which are known to be extremely sensitive to the part of the matrix included in the determination of relationships between the crystal field and the spin Hamiltonian parameters. At the same time, this theoretical method opens the possibilities to test a different approximate method, for example, the high-order perturbation method. Of course, our theoretical results remain to be checked by other more direct experiments.

IV. Conclusion

From the above studies, we have the following conclusions.

(i) The EPR and optical absorption spectra of Mn^{2+} ions in $CaCO_3$ have been studied by the complete energy matrices for a d^5 configuration ion in a trigonal ligand field. It is worth noting that the above theoretical study of EPR and optical absorption spectra provides powerful guidelines for future experimental studies aimed at pinpointing exactly how Mn enters into the $CaCO_3$ environment.

(ii) By solving the energy matrices, the zero-field splitting parameters b_2^0 and b_4^0 have been derived, and the theoretical values are found to be in good agreement with the experimental findings.

(iii) From the EPR calculation, local structure distortion parameters ΔR and $\Delta\theta$ for Mn^{2+} ions in $CaCO_3$ are determined. The results show that the local lattice structure of the $(MnO_6)^{10-}$ coordination complex for Mn^{2+} ions in the $CaCO_3$:Mn^{2+} system has a compressed distortion and the local lattice structure of the $CaCO_3$:Mn^{2+} system for Mn^{2+} ions in travertines and shells are obviously different from those in calcite single crystal. Moreover, the theoretical values of the zero-field splitting parameter b_4^0 for Mn^{2+} ions in travertines and shells are reported first. These parameters are of significance in broadening our understanding of the physical and chemical properties of $CaCO_3$. Of course, careful experimental investigations, especially electron nuclear double resonance (ENDOR) experiments, are required in order to clarify the local structure around the Mn^{2+} ions in the $CaCO_3$:Mn^{2+} system in detail.

Acknowledgment. The authors express their gratitude to Dr. Zhu Ben-Chao for many helpful discussions. This work was supported by the National Natural Science Foundation (No. 10374068) and the Doctoral Education Fund of Education Ministry (No. 20050610011) of China.

Appendix

Ligand Field Potential. The ligand field potential V_i in eq 4 can be written as[53]

$$V_i = \gamma_{00}Z_{00} + \gamma_{20}r_i^2Z_{20}(\theta_i, \phi_i) + \gamma_{40}r_i^4Z_{40}(\theta_i, \phi_i) + \gamma_{43}^c r_i^4 Z_{43}^c (\theta_i, \phi_i) + \gamma_{43}^s r_i^4 Z_{43}^s(\theta_i, \phi_i)$$

where r_i, θ_i, and φ_i are spherical coordinates of the ith electron. Z_{lm}, Z_{lm}^c and Z_{lm}^s are defined as

$$Z_{l0} = Y_{l0}$$

$$Z_{lm}^c = (1/\sqrt{2})[Y_{l,-m} + (-1)^m Y_{l,m}]$$

$$Z_{lm}^s = (i/\sqrt{2})[Y_{l,-m} - (-1)^m Y_{l,m}]$$

The $Y_{l,m}$ are the spherical harmonics. γ_{l0}, γ_{lm}^c, and γ_{lm}^s are associated with the local lattice structure around the d^5 configuration ion by the relations

$$\gamma_{l0} = -\frac{4\pi}{2l+1}\sum_{\tau=1}^{n}\frac{eq_\tau}{R_\tau^{l+1}}Z_{l0}(\theta_\tau, \varphi_\tau)$$

$$\gamma_{lm}^c = -\frac{4\pi}{2l+1}\sum_{\tau=1}^{n}\frac{eq_\tau}{R_\tau^{l+1}}Z_{lm}^c(\theta_\tau, \varphi_\tau)$$

$$\gamma_{lm}^s = -\frac{4\pi}{2l+1}\sum_{\tau=1}^{n}\frac{eq_\tau}{R_\tau^{l+1}}Z_{lm}^s(\theta_\tau, \varphi_\tau)$$

where θ_τ and φ_τ are angular coordinates of the ligand. τ and q_τ represent the τth ligand ion and its effective charge, respectively. R_τ denotes the impurity−ligand distance.

References and Notes

(1) Misra, S. K.; Andronenko, S. I. *J. Phys. Chem. B* **2004**, *108*, 9397.
(2) Zhecheva, E.; Stoyanova, R.; Alcántara, R.; Tirado, J. L. *J. Phys. Chem. B* **2003**, *107*, 4290.
(3) Jeschke, G. *J. Phys. Chem. B* **2000**, *104*, 8382.
(4) Mantel, C.; Baffert, C.; Romero, I.; Deronzier, A.; Pécaut, J.; Collomb, M. N.; Duboc, C. *Inorg. Chem.* **2004**, *43*, 6455.
(5) Dasgupta, J.; Tyryshkin, A. M.; Kozlov, Y. N.; Klimov, V. V.; Dismukes, G. C. *J. Phys. Chem. B* **2006**, *110*, 5099.
(6) Zong, X. H.; Zhou, P.; Shao, Z. Z.; Chen, S. M.; Chen, X.; Hu, B. W.; Deng, F.; Yao, W. H. *Biochemistry* **2004**, *43*, 11932.
(7) Keeble, D. J.; Loyo-Menoyo, M.; Furukawa, Y.; Kitamura, K. *Phys. Rev. B: Condens. Matter Mater. Phys.* **2005**, *71*, 224111.
(8) Diaconu, M.; Schmidt, H.; Pöppl, A.; Böttcher, R.; Hoentsch, J.; Klunker, A.; Spemann, D.; Hochmuth, H.; Lorenz, M.; Grundmann, M. *Phys. Rev. B: Condens. Matter Mater. Phys.* **2005**, *72*, 085214.
(9) Caudle, M. T.; Mobley, C. K.; Bafaro, L. M.; LoBrutto, R.; Yee, G. T.; Groy, T. L. *Inorg. Chem.* **2004**, *43*, 506.
(10) Zapart, W. *J. Phys. Chem. B* **2003**, *107*, 4208.
(11) Augustyniak-Jabłokow, M. A.; Krupska, A.; Krupski, M.; Yablokov, Y. V. *Inorg. Chem.* **2002**, *41*, 1348.
(12) Ozarowski, A.; Mcgarvey, B. R.; Sarkar, A. B.; Drake, J. E. *Inorg. Chem.* **1988**, *27*, 628.
(13) Smirnova, T. I.; Smirnov, A. I. *J. Phys. Chem. B* **2003**, *107*, 7212.
(14) Renault, J. P.; Verchère-Béaur, C.; Morgenstern-Badarau, I.; Yamakura, F.; Gerloch, M. *Inorg. Chem.* **2000**, *39*, 2666.

(15) Duboc-Toia, C.; Hassan, A. K.; Mulliez, E.; Ollagnier-de Choudens, S.; Fontecave, M.; Leutwein, C.; Heider, J. *J. Am. Chem. Soc.* **2003**, *125*, 38.
(16) Mantel, C.; Hassan, A. K.; Pécaut, J.; Deronzier, A.; Collomb, M. N.; Duboc-Toia, C. *J. Am. Chem. Soc.* **2003**, *125*, 12337.
(17) Wilson, J. C.; Wu, G.; Tsai, A.; Gerfen, G. J. *J. Am. Chem. Soc.* **2005**, *127*, 1618.
(18) Bertholon, I.; Hommel, H.; Labarre, D.; Vauthier, C. *Langmuir* **2006**, *22*, 5485.
(19) Benedetto, F. D.; Montegrossi, G.; Pardi, L. A.; Minissale, A.; Paladini, M.; Romanelli, M. *J. Magn. Reson.* **2005**, *177*, 86.
(20) Montegrossi, G.; Di Benedetto, F.; Minissale, A.; Paladini, M.; Pardi, L. A.; Romanelli, M.; Romei, F. *Appl. Geochem.* **2006**, *21*, 820.
(21) Barberis, G. E.; Calvo, R.; Maldonado, H. G.; Zarate, C. E. *Phys. Rev. B: Condens. Matter Mater. Phys.* **1975**, *12*, 853.
(22) Serway, R. A. *Phys. Rev. B: Condens. Matter Mater. Phys.* **1971**, *3*, 608.
(23) Wait, D. F. *Phys. Rev.* **1963**, *132*, 601.
(24) Slezak, A.; Lech, J.; Bojko, I. *Phys. Status Solidi A* **1979**, *54*, 755.
(25) Tennant, W. C. *J. Magn. Reson.* **1974**, *14*, 152.
(26) Zheng, W. C. *Physica B (Amsterdam, Neth.)* **1997**, *240*, 211.
(27) Yu, W. L.; Zhao, M. G. *J. Phys. C: Solid State Phys.* **1987**, *20*, 4647.
(28) Griffith, J. S. *The Theory of Transition-Metal Ions;* Cambridge University Press: London, 1964.
(29) Slater, J. C. *Quantum Theory of Molecules and Solids*; McGraw-Hill, New York, 1963; Vol. I.
(30) Zare, R. N. *Angular Momentum;* John Wiley & Sons: New York, 1988.
(31) Newman, D. J.; Urban, W. *Adv. Phys.* **1975**, *24*, 793.
(32) Abragam, A.; Bleaney, B. *Electron Paramagnetic Resonance of Transition Ions;* Clarendon Press: Oxford, 1970.
(33) Stevens, K. W. H. *Proc. Phys. Soc., London* **1952**, *65*, 209.
(34) Marshall, S. A.; Serway, R. A. *Phys. Rev.* **1968**, *171*, 345.
(35) Garribba, E.; Micera, G. *Magn. Reson. Chem.* **2006**, *44*, 11.
(36) Newman, D. J.; Ng, B. *Rep. Prog. Phys.* **1989**, *52*, 699.
(37) Vleck, J. H. V. *Phys. Rev.* **1932**, *41*, 208.
(38) Zhao, M. G.; Bai, G. R.; Jin, H. C. *J. Phys. C: Solid State Phys.* **1982**, *15*, 5959.
(39) L. L. L., Jr. *J. Chem. Phys.* **1966**, *45*, 3611.
(40) Cheng, L.; Sturchio, N. C.; Bedzyk, M. J. *Phys. Rev. B: Condens. Matter Mater. Phys.* **2001**, *63*, 144104.
(41) Pappalardo, R. *J. Chem. Phys.* **1960**, *33*, 613.
(42) Van, E. W.; Haas, C. *Phys. Status Solidi B* **1975**, *70*, 517.
(43) Ronda, C. R.; Siekman, H. H.; Haas, C. *Physica B* **1987**, *144*, 331.
(44) Newman, D. J.; Siegel, E. *J. Phys. C: Solid State Phys.* **1976**, *9*, 4285.
(45) Curie, D.; Barthon, C.; Canny, B. *J. Chem. Phys.* **1974**, *61*, 3048.
(46) Kuang, X. Y.; Zhang, W.; Morgenstern-Badarau, I. *Phys. Rev. B: Condens. Matter Mater. Phys.* **1992**, *45*, 8104.
(47) Blanchard, S. C.; Chasteen, N. D. *J. Phys. Chem.* **1976**, *80*, 1362.
(48) Prasuna, C. P. L.; Narasimhulu, K. V.; Gopal, N. O.; Rao, J. L.; Rao, T. V. R. K. *Spectrochim. Acta. A* **2004**, *60*, 2305.
(49) Narasimhulu, K. V.; Rao, J. L. *Spectrochim. Acta, Part A* **2000**, *56*, 1345.
(50) Raju, C. L.; Narasimhulu, K. V.; Gopal, N. O.; Rao, J. L.; Reddy, B. C. V. *J. Mol. Struct.* **2002**, *608*, 201.
(51) Naidu, Y. N.; Rao, J. L.; Lakshman, S. V. J. *Polyhedron* **1992**, *11*, 663.
(52) Polikreti, K.; Maniatis, Y. *Atmos. Environ.* **2004**, *38*, 3617.
(53) Hutchings, M. T. *Solid State Phys.* **1964**, *16*, 227.